

Strong Coupling in Semiconductor Hyperbolic Metamaterials

Prashant Shekhar¹ and Zubin Jacob¹

¹*Department of Electrical and Computer Engineering,
University of Alberta, Edmonton, AB T6G 2V4, Canada*

Nanoscale light-matter interaction in the weak coupling regime has been achieved with unique hyperbolic metamaterial modes possessing a high density of states. Here, we show strong coupling between intersubband transitions (ISBTs) of a multiple quantum well (MQW) slab and the bulk polariton modes of a hyperbolic metamaterial (HMM). These HMM modes have large wavevectors (high- k modes) and are normally evanescent in conventional materials. We analyze a metal-dielectric practical multilayer HMM structure consisting of a highly doped semiconductor acting as a metallic layer and an active multiple quantum well dielectric slab. We observe delocalized metamaterial mode interaction with the active materials distributed throughout the structure. Strong coupling and characteristic anticrossing with a maximum Rabi splitting (RS) energy of up to 52 meV is predicted between the high- k mode of the HMM and the ISBT, a value approximately 10.5 times greater than the ISBT linewidth. The predicted strong coupling can be experimentally verified through the angle resolved spectroscopy of the multiple high- k modes which form a series of high- k -ISBT polaritons. The scalability and tunability of the RS energy in an active semiconductor metamaterial device have potential applications in quantum well infrared photodetectors and intersubband light-emitting devices.

I. INTRODUCTION

Metamaterials, artificial media synthesized from nanostructured building blocks, have an increasing set of applications such as nano-waveguiding, sensing, subwavelength-imaging and cloaking [1–7]. Recently they have shown promise for engineering nanoscale light-matter interaction opening the possibility of quantum applications [8, 9]. In particular, multiple groups have studied modified spontaneous emission of quantum emitters in the weak coupling limit (irreversible regime) [10, 11]. Governed by Fermi's golden rule, the emitters spontaneously emit light into the engineered channels provided by the metamaterials. The two signatures of the modified spontaneous emission are the reduced lifetime and altered emission pattern [12].

Strong coupling, unlike the weak coupling limit, relies on the back-action between the emitter and the metamaterial to create coherent states between light and matter [13–15]. The lifetime of the mode and the radiative lifetime of the emitter is critical to achieve the strong interaction between light and matter. The characteristics of strong coupling is often ascertained through the spectral signatures in either the absorption or emission of the coupled emitter-environment system [16].

Microcavities and photonic crystals have been studied extensively with both weakly coupled and strongly coupled single emitters. The weak coupling regime has been used to engineer the spontaneous decay rate of an emitter by coupling it to the resonant modes of the structure [17–20]. Strongly coupled light-matter states have also been demonstrated in such systems [13–15, 21, 22]. Although these structures are able to effectively couple light and matter, they are wavelength sized diffraction limited structures. Additionally, the resonant nature of the modes limits their bandwidth of operation. Propagating surface-plasmon polaritons on metals are a suitable can-

didate for subwavelength radiative decay engineering [23] or strong coupling [24–26] while low mode volume surface plasmons (eg: 1D nanowire) can be used for broadband coupling between emitters and plasmons [27].

A natural question then arises whether delocalized plasmonic modes which lead to collective metamaterial behavior can show effects such as coherence and strong coupling. Resonant metamaterials have shown strong coupling to quantum well emitters proving that even lossy modes can enter the strong coupling regime [28]. Here, we introduce strong coupling at the nanoscale with non-resonant hyperbolic metamaterials (HMMs). HMMs are a special class of metamaterial with an extremely anisotropic dielectric tensor resulting in a hyperbolic dispersion for the structure [29, 30]. This unique hyperbolic dispersion leads to novel phenomena in HMMs such as the ability to support subwavelength modes as well as a broadband enhancement to the photonic density of states [7, 10]. HMMs have shown promise for applications in the weak coupling regime [31], specifically in the field of radiative decay engineering to produce broadband single-photon sources [9–11, 32, 33]. The main challenges to be overcome are the efficient out-coupling of the metamaterial modes and metallic losses [33, 34].

In this paper, we predict strong coupling behaviour with the subwavelength modes of an HMM. The proposed structure consists of an HMM with embedded active components in the form of quantum wells. We show that such strong coupling effects can persist even in the presence of metallic losses. We provide a practical semiconductor superlattice design for our metamaterial consisting of highly doped n^+ -InGaAs as the metallic building block and embedded multiple quantum wells ($\text{Al}_{0.35}\text{Ga}_{0.65}\text{As}/\text{GaAs}$). The proposed structure can be fabricated by molecular beam epitaxy and the predicted effect can be isolated in experiment through angle resolved spectroscopy of the quantum well absorption.

This work presents the initial steps to realizing novel mixed and coherent states between metamaterial modes and embedded emitters. In the limit of many quantum emitters in a system (eg: multiple quantum wells, thin film of dye molecules or quantum dots), strong coupling behaviour in metamaterial structures can be treated semiclassically. However, single emitter systems can show anharmonic effects which require a fully quantized treatment [35–37]. The same holds true in the weak coupling regime where effects such as antibunching of light from isolated emitters cannot be treated classically [38]. Experimental verification of strong coupling between quantum wells and hyperbolic metamaterial states should lead to avenues of realizing strong coupling with single emitters and metamaterials.

II. HYPERBOLIC METAMATERIALS

A. High- k Modes

Hyperbolic Metamaterials (HMMs) are artificial uniaxial materials with an extremely anisotropic dielectric tensor. The extreme anisotropy requires the components of the permittivity to be defined such that $\epsilon_{xx} = \epsilon_{yy}$ and $\epsilon_{zz} \times \epsilon_{xx} < 0$. The unique electromagnetic response gives rise to an unconventional dispersion relation for extraordinary waves in a uniaxial material [31]:

$$\frac{k_x^2 + k_y^2}{\epsilon_{zz}} + \frac{k_z^2}{\epsilon_{xx}} = \left(\frac{\omega}{c}\right)^2 \quad (1)$$

The term hyperbolic is used to describe the hyperbolic dispersion of the isofrequency surface of the HMM as opposed to the spherical or ellipsoidal isofrequency surfaces seen in conventional materials.

This hyperbolic behaviour of the isofrequency surface can be defined for two separate regimes, giving rise to two types of HMMs. Type I HMMs have a single negative component of the dielectric tensor in a direction normal to the metamaterial surface ($\epsilon_{zz} < 0$) whereas Type II HMMs have two negative components of the uniaxial dielectric tensor that are planar to the metamaterial surface ($\epsilon_{xx} < 0, \epsilon_{yy} < 0$) [31].

The unbounded hyperboloid isofrequency surfaces, seen in Figure 1, display the ability of the Type I and Type II HMMs to support waves with large wavevectors or high- k waves. These high- k waves are normally evanescent in conventional media with bounded (spherical or ellipsoidal) isofrequency surfaces. However, these high- k waves have the ability to propagate in the HMM as a result of its characteristic hyperbolic dispersion [4, 5, 7].

B. Semiconductor HMMs

One realization of a hyperbolic metamaterial involves a planar multilayer structure with alternating subwavelength metal-dielectric layers [4, 5]. The high- k modes

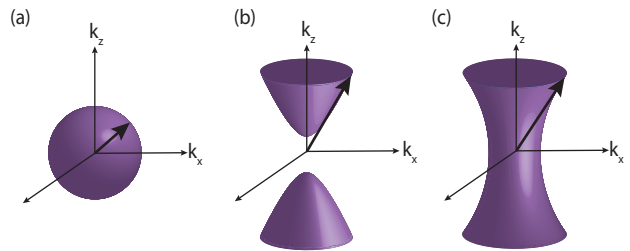


FIG. 1: k -space topology. (a) Spherical isofrequency surface for an isotropic dielectric. (b) Hyperboloid isofrequency surface for a uniaxial medium with an extremely anisotropic dielectric response (Type I HMM: $\epsilon_{zz} < 0, \epsilon_{xx}, \epsilon_{yy} > 0$) (c) Hyperboloid isofrequency surface for an extremely anisotropic uniaxial medium with two negative components of the dielectric tensor (Type II HMM: $\epsilon_{xx}, \epsilon_{yy} < 0, \epsilon_{zz} > 0$). The (b) Type I and (c) Type II metamaterials can support waves with infinitely large wavevectors in the effective medium limit.

of the system arise from the near-field coupling of the surface plasmon polaritons (SPPs), excited with incident p-polarized light, at each of the metal-dielectric interfaces in the structure. The high- k modes are the Bloch modes of the metal-dielectric superlattice. [9, 10].

The building blocks of HMMs can be composed of metals such as silver and gold that exhibit plasmonic resonances near their plasma frequency. However, the high plasma frequency of these metals which usually lie in the ultraviolet (UV) make them very reflective in the infrared (IR). Semiconductors allow for the ability to harness these plasmonic resonances in the mid-IR [39]. Specifically, the metal in a conventional metal-dielectric HMM can be replaced with a degenerately doped semiconductor to create a new class of hyperbolic metamaterials. These semiconductor HMMs, aside from their ability to support high- k states in the near-IR and mid-IR, have the distinct advantage of being able to tune their plasma frequencies by variation of their electron doping density.

In this paper, we analyze a planar active semiconductor HMM composed of alternating layers of a multiple quantum well (MQW) slab and a degenerately doped semiconductor functioning as a plasmonic metal in the infrared. The MQW slab is composed of layered semiconductors to create a series of quantum wells. We show that the high- k waves of the semiconductor HMM strongly couple to intersubband transitions (ISBTs) present in the MQW slab as a result of quantum confinement effects (Figure 2). Semiconductor HMMs have potential applications in quantum well infrared photodetectors and tunable intersubband light-emitting devices [40]. We emphasize that the proposed semiconductor super-lattice can be fabricated by lattice matched molecular beam epitaxy techniques [39].

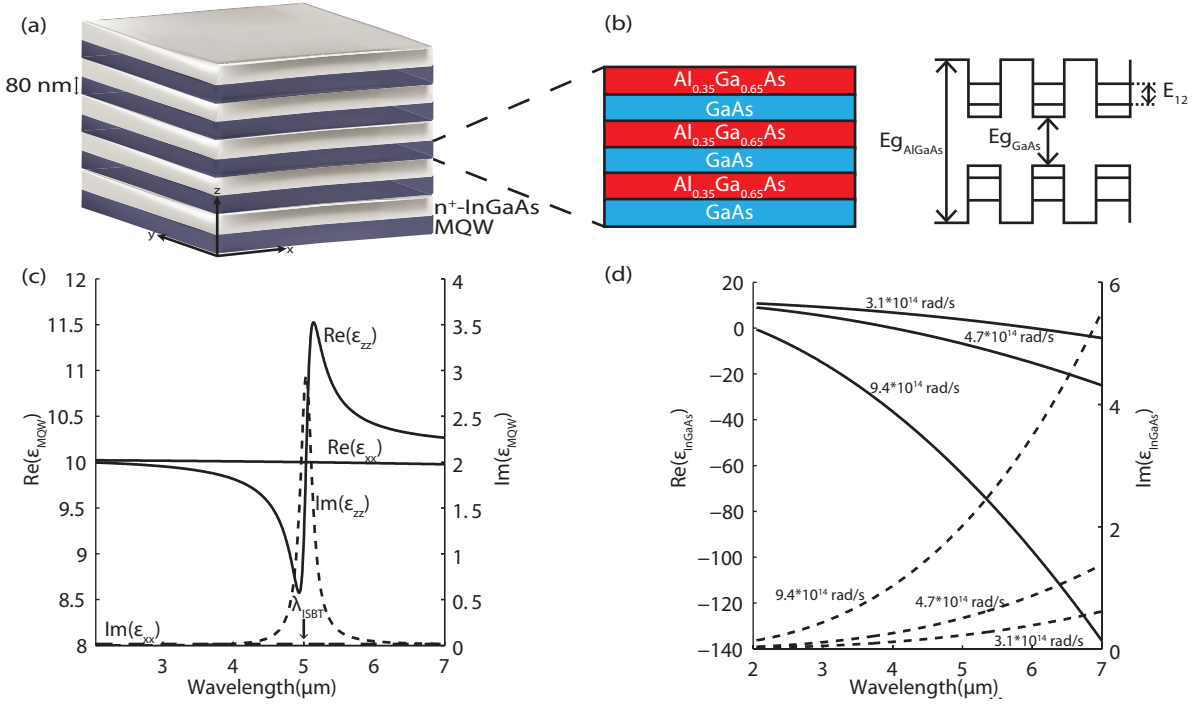


FIG. 2: (a) Multilayer realization of a semiconductor HMM. The structure consists of alternating 80 nm thick subwavelength layers of a dielectric MQW slab and degenerately doped n^+ -InGaAs. The extreme anisotropy of the structure results in a hyperbolic isofrequency surface. (b) Quantum well structure of the MQW slab. (c) Perpendicular and parallel permittivities of the purely dielectric MQW slab. The resonance at a wavelength of $\lambda_{ISBT} = 5\mu\text{m}$ corresponds to the energy of the intersubband transition in a single quantum well of the MQW structure. (d) Dispersion of the n^+ -InGaAs semiconductor layer at different plasma frequencies. The negative permittivity of the InGaAs layer (metallic response) is required in order to realize a hyperbolic isofrequency surface for the semiconductor HMM.

C. Effective Medium Theory for a Uniaxial Medium

In this section we will look at the definition of a multilayer structure as an effective uniaxial medium. Effective medium theory (EMT) can be used when the wavelength of operation is much larger than the unit cell size of the metamaterial. The permittivity of both the parallel (ϵ_{\parallel}) and perpendicular (ϵ_{\perp}) components of the dielectric tensor can be determined by averaging the displacement field and applying the electromagnetic boundary conditions:

$$\epsilon_{\parallel} = \epsilon_2 \rho + (1 - \rho) \epsilon_1 \quad (2)$$

$$\frac{1}{\epsilon_{\perp}} = \frac{\rho}{\epsilon_2} + \frac{1 - \rho}{\epsilon_1} \quad (3)$$

$$\epsilon_{eff} = \begin{pmatrix} \epsilon_{\parallel} & 0 & 0 \\ 0 & \epsilon_{\perp} & 0 \\ 0 & 0 & \epsilon_{\perp} \end{pmatrix} \quad (4)$$

Here ϵ_1 and ϵ_2 represent the permittivities of the first and second alternating layers of a multilayer structure and ϵ_{eff} is the effective dielectric constant of the uniaxial slab. For the case of a semiconductor HMM we consider $\epsilon_1 > 0$ (dielectric) and $\epsilon_2 < 0$ (metallic) in order to

achieve the hyperbolic dispersion for the structure [4, 5]. The fill fraction, $\rho = d_2 / (d_1 + d_2)$, is the weighted fraction of the thickness of layer 2 (d_2) to the total thicknesses of layer 1 (d_1) and layer 2 of the multilayer structure.

D. Dielectric Component: Effective Medium Theory for the Multiple Quantum Well Slab

In this paper, we look at a semiconductor HMM with an MQW slab acting as an active dielectric layer. The MQW slab itself is modeled with an EMT approach. Previous analytic and experimental work have shown the validity of using EMT to model the behaviour of MQW structures [40, 41]. The quantum well thickness, L_{QW} (6 nm), and the MQW period, L_{MQW} (20 nm), are much smaller than the wavelength of the incident infrared radiation and the wells themselves are assumed to be quantum mechanically isolated from each other. This is the first scale of homogenization for the 80 nm thick MQW structure. We will see, in Section III, that a second homogenization between the MQW and the metallic components will be performed to describe the overall metal-dielectric effective medium. The MQW slab is composed of alternating subwavelength layers of $\text{Al}_{0.35}\text{Ga}_{0.65}\text{As}$ and GaAs to form the multiple quantum

wells. Here, $\text{Al}_{0.35}\text{Ga}_{0.65}\text{As}$, with its larger bandgap relative to GaAs, creates the barriers for the structure (Figure 2(b)).

MQWs show free electron movement in the plane parallel to the surface (the x-y plane) and quantum confinement, with possible ISBTs, in the the plane normal to the interface (z-direction). This quasi-two-dimensional electron gas can be modeled with an anisotropic dielectric tensor with a uniaxial crystal symmetry. The permittivity of the MQW slab, in the plane parallel to the interface, is effectively characterized by a Drude model [40, 42]:

$$\epsilon_{xx}^d = \epsilon_{yy}^d = \epsilon_y - \frac{\omega_{p,mqw}^2}{\omega^2 + i\omega\gamma_1} \quad (5)$$

Permittivity in the plane perpendicular to the MQW interface is characterized with a Lorentzian Oscillator Model in order to incorporate the quantum confinement effects of the structure, specifically the resonance at the ISBT energy [40, 42]:

$$\epsilon_{zz}^d = \frac{1}{\epsilon_z} - \frac{\frac{\omega_{p,mqw}^2 f_{12}}{2\omega\gamma_2 \epsilon_{well}}}{\frac{E_{12}^2 - \hbar^2 \omega^2}{2\hbar^2 \gamma_2 \omega} - i} \quad (6)$$

Here, ϵ_y and ϵ_z represent the mean effective background dielectric constant and are given as $\epsilon_y = (1 - L_{QW}/L_{MQW})\epsilon_{barrier}$ and $\epsilon_z^{-1} = (1 - L_{QW}/L_{MQW})/\epsilon_{barrier} + (L_{QW}/L_{MQW})/\epsilon_{well}$, with $\epsilon_{barrier}$ (9.88) and ϵ_{well} (10.36) representing the undoped background dielectric constant for the barrier and well respectively [42]. $\omega_{p,mqw} = (n_s e^2 / m \epsilon_0 L_{MQW})^{1/2}$ is the plasma frequency for the system where e is the elementary charge of the electron, ϵ_0 is the vacuum permittivity constant, $m^* = 0.0665m$ is the effective mass of the electron, where m is the mass of an electron in vacuum, and $n_s = 1.5 \times 10^{12} \text{cm}^{-2}$ is the areal electron density per quantum well. f_{12} corresponds to the oscillator strength of the resonance which depends on the transition energy of the ISBT, the effective mass of the electron and the intersubband dipole matrix element. E_{12} is the ISBT transition energy, which, for the parameters established is set to be equal to $\lambda_{ISBT} = 5\mu\text{m}$ (0.2480 eV). $\gamma_1 = \gamma_2$ is the electron scattering rate given as $7.596 \times 10^{12} \text{s}^{-1}$ [40].

The superscript d in the definitions of both the parallel and perpendicular permittivities given in Equation 5 and Equation 6 respectively, is used to emphasize that the MQW slab is purely dielectric as we are operating above the plasma frequency ($\omega_{p,mqw}$) of the MQW slab. The dispersion for the MQW slab can be seen in Figure 2(c).

One will note that the properties of the ISBT are only present in the perpendicular (ϵ_{zz}) component of the dielectric tensor (Equation 6) as the ISBT can only be excited with electric fields polarized in the growth direction (z-direction) of the slab. This is due to the fact that

wavefunctions of each subband are also bound in the z-direction and thus, due to orthogonality conditions, transitions between states require absorption from z-polarized E-fields. S-polarized light will have no z-component of the electric field, and thus p-polarized incidence is required to see effects of the ISBTs in the semiconductor HMM. Note that the ISBT resonance is compatible with the high-k modes of the metamaterials since both occur only for p-polarized light.

E. Metallic Component: Degenerately Doped InGaAs Layer

The MQW slab is purely dielectric such that $\text{Re}(\epsilon_{xx}^d) > 0$ and $\text{Re}(\epsilon_{zz}^d) > 0$. Thus, as outlined in Section II A, a separate metallic layer is needed to achieve hyperbolic dispersion in a super-lattice geometry. The plasmonic metal in this case can be a degenerately doped InGaAs (n^+ -InGaAs) semiconductor with $\text{Re}(\epsilon_{InGaAs}) < 0$. The n^+ -InGaAs layer is assumed to be isotropic and approximated with Drude-like behaviour [39]:

$$\epsilon_{InGaAs} = \epsilon_{b,InGaAs} \left(1 - \frac{\omega_{p,InGaAs}^2}{\omega^2 + i\omega\gamma} \right) \quad (7)$$

Here, $\epsilon_{b,InGaAs}$ is the background dielectric set at 12.15, γ is the electron scattering rate set to $1 \times 10^{13} \text{s}^{-1}$ and $\omega_{p,InGaAs}$ is the plasma frequency. Figure 2(d) shows the dispersion of ϵ_{InGaAs} at different plasma frequencies of the semiconductor. For the analysis in this paper, we set $\omega_{p,InGaAs} = 9.43 \times 10^{14} \text{rad/s}$ to best interact with the MQW slab. For experimental considerations, doping to high concentrations and pushing the plasma frequency to the near-infrared is a significant challenge. The key is to achieve the lorentzian response of the MQW in the bandwidth of the metallic behaviour for InGaAs. One approach to tune the response of the MQW is through the control of quantum well thickness and period to shift the ISBT energy to the optimal wavelength.

F. Basis of Strong Coupling: Semi-classical Perspective

In the previous section we presented the semiconductor based active dielectric layer and metallic layer needed for achieving multilayer hyperbolic metamaterials. Before we present the characteristics of strong electromagnetic interactions in this active metamaterial, we discuss the semiclassical theory of strong coupling for the case of hyperbolic media.

Strong coupling has been a key area of interest over the past decade for its potential in creating coherent and entangled states between light and matter [13–15, 21, 22]. It is the result of a large interaction between two distinct resonances within a system. In a semiconductor HMM,

for example, strong light-matter coupling is possible between the Lorentzian resonance of the ISBTs and the high- k modes of the structure. Strong coupling between two resonances results in a typical polaritonic dispersion and a collective excitation unlike the weak coupling limit [43]. Specifically, in the strong coupling regime, the strength of coupling between the two resonances is greater than the sum of the damping rates of both resonators. We will first observe how to semi-classically derive strong coupling behaviour between a Lorentzian resonance, such as an ISBT, and a high- k mode of an HMM. We can then extend this analysis to our understanding of the strong coupling interaction as described in Section II G.

Using the dispersion outlined in Equation 1 we define the energy for a high- k mode in a semiconductor HMM as:

$$E_{high-k}^2(q) = \hbar^2 c^2 \left(\frac{q^2}{\epsilon_{zz}} + \frac{k_z^2}{\epsilon_{xx}} \right) \quad (8)$$

Here $q^2 = k_x^2 + k_y^2$, ϵ_{zz} and ϵ_{xx} are the perpendicular and parallel permittivity respectively, and k_z is the wavevector normal to the interface. We now assume a Lorentzian ISBT resonance is added to the HMM in the form of a low loss Lorentzian Oscillator model. The dispersion given in Equation 8 can now be rewritten as follows [41]:

$$\left(\frac{\hbar^2 c^2 q^2}{E^2 - \frac{\hbar^2 c^2 k_z^2}{\epsilon_{xx}}} \right) = \epsilon_{zz} + \frac{C}{E_{ISBT}^2 - E^2} \quad (9)$$

Note that we are only adding the ISBT resonance to the perpendicular (ϵ_{zz}) component of the permittivity since the absorption requires the field component perpendicular to the growth axis (Section II D). C is the constant representative of the oscillator strength of the resonance and E_{ISBT} is the ISBT energy. In the regime of strong coupling, we assume that the resonant energy (E_{ISBT}) and the high- k mode energy (E_{high-k}) become degenerate such that $E \approx E_{high-k} \approx E_{ISBT}$ [41]. Taking this into account and solving for E to determine the resultant dispersion of the system from Equation 9 we arrive at the following:

$$E_{U,L}(q) = \frac{E_{high-k}(q) + E_{ISBT}}{2} \pm \frac{\sqrt{4(\Gamma)^2 + (E_{high-k}(q) - E_{ISBT})^2}}{2} \quad (10)$$

Equation 10 shows the formation of the resultant upper and lower polariton branches of the dispersion in the regime of strong coupling. The magnitude of the splitting between the upper and lower branches of the dispersion is proportional to $\Gamma^2 = \frac{C\hbar^2 c^2 q^2}{4\epsilon_{zz}^2 E_{ISBT} E_{high-k}}$ and is much larger than the ISBT linewidth if the resonances

are strongly coupled. The polaritonic dispersion emphasizes the mixing of the states between the two resonances in the strong coupling regime.

G. Rabi Splitting in Semiconductor HMMs

We now define the strong coupling behaviour in the semiconductor HMM through the Rabi splitting (RS) energy. The RS energy denotes the energy level splitting between two strongly coupled resonances within a system. The semiconductor HMM, as derived classically in Section II F, displays strong coupling phenomena when the energy of the ISBT and the high- k mode become degenerate [44]. The explicit regime of strong coupling occurs when the magnitude of the rs energy is greater than the sum of the linewidth of the high- k mode and the radiative broadening of the ISBT resonance [45–47]. This results, as expected, in a mixed state between the two resonances of the system leading to a high- k -ISBT polariton.

The resultant dispersion and, more importantly, the magnitude of the splitting energy of the high- k -ISBT polariton can be accomplished by describing the coupling between two oscillators with a 2×2 matrix Hamiltonian given by [46, 47]:

$$H = \begin{pmatrix} E_{ISBT} & \frac{\hbar\Omega}{2} \\ \frac{\hbar\Omega}{2} & E_{high-k} \end{pmatrix} \quad (11)$$

Here, E_{ISBT} and E_{high-k} represent the respective energy dispersions of each of the resonances, specifically the ISBT and the high- k mode respectively. For the systems observed in this paper, the ISBT resonance is assumed to be at one particular energy across all values of the in-plane wavevector (k_x). The coupling matrix term proportional to $\hbar\Omega$ is representative of the Rabi splitting energy of the system.

We solve the eigenvalue problem for the matrix given in Equation 11 to determine the dispersion of the system [46, 47]:

$$E_{U,L}(q) = \frac{E_{high-k}(q) + E_{ISBT}}{2} \pm \frac{\sqrt{4(\frac{\hbar\Omega}{2})^2 + (E_{high-k}(q) - E_{ISBT})^2}}{2} \quad (12)$$

Here we see solutions for the upper and lower branch of the polaritons observed from strong coupling interaction between the two resonances. Comparing Equation 10 and Equation 12, we clearly note that the RS ($\hbar\Omega$) has taken the place of the semi-classical splitting energy (Γ) in Equation 10. We can now define our splitting energy for the system with the known RS energy, $\hbar\Omega$. Equation 12 assumes that $\hbar\Omega$, is much larger than the radiative broadening of the ISBT, as is the case in the strong coupling regime.

For the analysis done in this paper, we use Equation 12 to determine the semiclassical Rabi splitting energy of the semiconductor HMM system. The semiclassical approach is warranted as the system does not deal with single emitters, but a multitude of emitters in the MQW layers. In Section III and Section IV we will numerically determine the dispersion of the proposed semiconductor HMM as both an effective medium and a practical multilayer structure. The numerical results will then be compared to the analytical dispersion given by Equation 12 to determine if strong coupling is present in the system.

III. STRONG COUPLING IN TYPE II SEMICONDUCTOR HMMS: EFFECTIVE MEDIUM APPROACH

We now analyze the strong coupling interaction between the Type II high- k modes of a semiconductor HMM and the ISBTs of the structure using effective medium theory. As outlined in Section II C, metamaterials interacting with incident radiation at wavelengths much longer than the individual layer thicknesses of the structure can be homogenized and treated as an effective medium.

The semiconductor HMM consists of a series of alternating subwavelength semiconductor layers (Figure 2(a)). Here, we show the transmission spectra of the MQW/InGaAs multilayer structure considered as an effective medium slab. We use the homogenized EMT equations for a uniaxial medium (Section II D):

$$\epsilon_{\parallel} = \epsilon_{InGaAs}\rho + (1 - \rho)\epsilon_{xx}^d \quad (13)$$

$$\frac{1}{\epsilon_{\perp}} = \frac{\rho}{\epsilon_{InGaAs}} + \frac{1 - \rho}{\epsilon_{zz}^d} \quad (14)$$

ϵ_{xx}^d and ϵ_{zz}^d are the parallel and perpendicular effective medium permittivities for the MQW slab respectively and ϵ_{InGaAs} is the permittivity of n⁺-InGaAs. Note that the permittivities of the MQW slab (ϵ_{xx}^d and ϵ_{zz}^d) are both positive while the InGaAs permittivity (ϵ_{InGaAs}) is negative to achieve the hyperbolic dispersion of the slab. The fill fraction, ρ , is assumed to be 0.5 throughout the paper as both the MQW and n⁺-InGaAs have equal layer thicknesses.

The homogenized dispersions shown in Figure 3 are plotted for wavelengths larger than the plasma frequency and outline the transitions from the Type I region to the Type II region of the HMM. This shift in the dispersion of the metamaterial, where the two-sheeted hyperboloid (Type I) transitions to the single-sheeted hyperboloid (Type II), is a special case of an optical topological transition (OTT) [48]. In Figure 3(a) we can see the resonance in the permittivity as result of the topological transition at $\lambda_{OTT} \approx 2.8 \mu\text{m}$.

Knowledge of λ_{OTT} gives useful insight into the behaviour of our hyperbolic metamaterial for different regions of the electromagnetic spectrum. The semiconductor HMM is in the Type I region up to $\lambda_{OTT} \approx 2.8 \mu\text{m}$ after which point larger wavelengths correspond to a Type II HMM. Furthermore, the resonance in ϵ_{\perp} at $\lambda_{ISBT}=5 \mu\text{m}$ (inset Figure 3(a)) corresponds to the ISBT resonance of the structure in the Type II region. The imaginary component of the permittivity represents the material absorption. We can see in the inset of Figure 3(a) that the imaginary permittivity is peaked at $\lambda_{ISBT}=5 \mu\text{m}$. Note that if the ISBT energy is tuned away from the range of wavelengths shown here, or is turned off completely, the resonance at λ_{ISBT} would not appear in the dispersion of the perpendicular permittivity (ϵ_{\perp}).

We have established the dispersive properties of the permittivities for our homogenized uniaxial medium. We now use the dispersions shown in Figure 3 and the transfer matrix method to evaluate the transmission through an 800 nm thick homogenized MQW-InGaAs slab (Figure 4). Figure 4(a) shows the high- k modes for a semiconductor HMM with the ISBT resonance tuned away from the observed modes. Clear regions of the Type I and Type II modes are distinguishable and are in correspondence with the EMT parameters of Figure 3. We also note that due to the hyperbolic dispersion the in plane wavevector (k_x) is unbounded in this EMT limit, and high- k modes up to wavevector magnitudes approaching infinity will be observed [31, 32].

Closer examination of Figure 4 also reveals a distinct cut-off region for the Type II modes where there is no transmission through the metamaterial in k -space. The metamaterial is highly metallic and thus extremely reflective in the cut-off region. The appearance of high- k modes starts at the k_{min} point where conditions are satisfied to support the high- k modes for the structure [31].

We now turn our attention to Figure 4(b) which shows the transmission spectra through the same semiconductor HMM shown in Figure 4(a) except with the ISBT resonance now tuned to $\lambda_{ISBT} = 5 \mu\text{m}$. Each high- k mode now couples with ISBT resonance of the metamaterial showing anticrossing behaviour at the ISBT wavelength (λ_{ISBT}). Subsequently, the high- k mode gains a typical polariton like dispersion as a result of the strong coupling. The mixed state between the high- k mode and the ISBT leads to the creation of an high- k -ISBT polariton. Strong coupling zones, whether it be particular wavevector regions or energies, can be assigned by tuning the ISBT energy or the dispersion profile of the modes [44]. Both of these parameters can be tuned by the quantum well thickness and period as well as the doping density of the semiconductors in the structure. Note, however, that the dispersion of the permittivity and the losses of the systems would need to be taken into consideration in order to ensure that conditions for strong coupling are met.

Now that we have qualitatively observed the strong coupling between the high- k mode and the ISBT (Figure 4(b)) we can determine the extent of the interaction

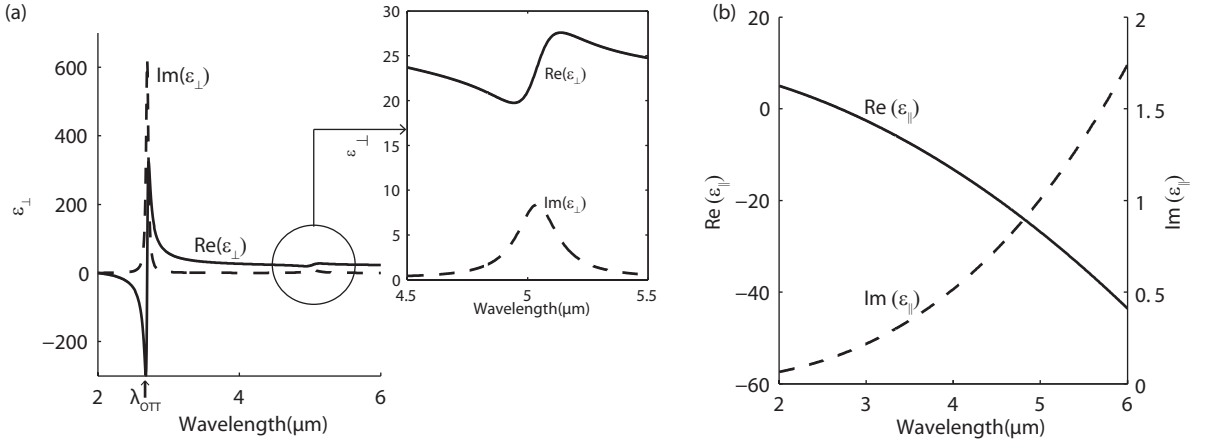


FIG. 3: (a) Perpendicular and (b) parallel dispersions for the homogenized MQW-InGaAs structure given by Equation 13 and Equation 14 respectively. A clear transition from the Type I to the Type II region is noticed at a wavelength of $\lambda_{OTT} \approx 2.8 \mu\text{m}$ where the parallel and perpendicular components of the permittivity both change sign. A smaller resonance at $\lambda_{ISBT} = 5 \mu\text{m}$ is shown in the inset of (a) which corresponds to the intersubband transition energy of the structure.

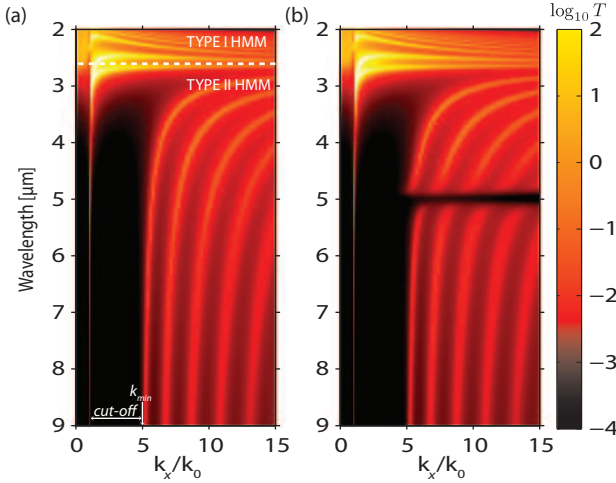


FIG. 4: Transmission (log scale) through an 800 nm thick homogenized MQW-InGaAs slab simulated with the transfer matrix method. (a) Type I and Type II high- k modes of the slab with intersubband transitions (ISBTs) of the slab tuned away from the mode energies. (b) Strong coupling between the ISBT and Type II modes of the slab at $\lambda_{ISBT} = 5 \mu\text{m}$. A series of high- k -ISBT polaritons are formed. In both (a) and (b) the structure supports high- k modes up to infinitely large wavevectors. The cut-off region indicates the wavevectors for which no transmission is allowed through the slab until k_{min} , indicating the smallest wavevector for the 1st high- k mode in the defined wavelength range. k_0 is the free-space wavevector.

by measuring the splitting energy of the polariton. The magnitude of splitting observed can be quantified by extracting a specific high- k -ISBT polariton from the dispersions in Figure 4(b) and matching it to the analytical expression of Equation 12. The RS energy in Equation 12 can be used as a fitting parameter to achieve the best fit between the numerical results and the analytical ex-

pression. The 4th high- k ISBT polariton (for the region lying between 12-14 k_x/k_0) is extracted, as seen in Figure 5, and plotted in conjunction with the analytical expression with a fitting parameter for the RS energy at $\hbar\Omega = 38\text{meV}$.

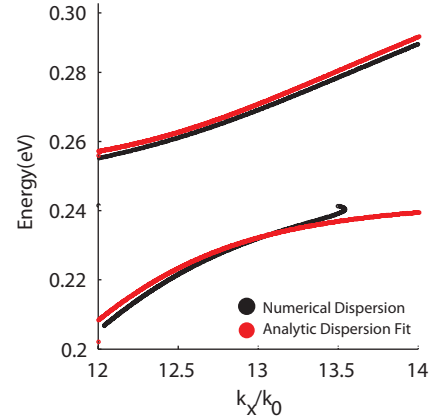


FIG. 5: Analytic (Equation 12) and numerical dispersions for the extracted 4th high- k -ISBT polariton shown in Figure 4(b). The magnitude of the splitting energy is determined by using the RS energy as a fitting parameter in the analytical expression to match the numerical results. The fitting parameter $\hbar\Omega = 38\text{meV}$ is used in the analytical expression.

Figure 5 provides a visual of the numerical simulation and analytic model for the strong coupling in the semiconductor HMM. There is a strong correlation between the numerical transfer matrix dispersion and the 2 level model analytic dispersion (Equation 12) using the RS energy as a fitting parameter. This allows us to make a good approximation of the splitting energy for the 4th high- k -ISBT polariton. However, we note that the lower branch starts back-bending at higher values of the in-

TABLE I: Rabi splitting (RS) energy between Type II HMM Modes and the ISBT for the 800 nm thick homogenized MQW-InGaAs slab shown in Figure 4. The magnitude of the RS is decreasing with increasing Type II mode number and wavevector magnitude (k_x/k_0).

High- k ISBT	k_x/k_0 Bounds	RS Energy ($\hbar\Omega$) [meV]
1	5-6.6	45
2	6.9-8.7	41
3	9-11.2	39
4	12-15	38

plane wavevector (k_x) in the simulated curve. This can be attributed to the loss and imperfections of the system, showing behaviour related to lossy polaritons. The analytical expression (Equation 12) does not take the back-bending behaviour due to such losses into account. However, the magnitude of the RS energy determined for the high- k -ISBT polaritons is still a valid approximation as seen with the strong correlation between the simulated and analytic results.

The approximated RS energies for all the high- k -ISBT polaritons (Table I) show that the maximum splitting occurs with the first polariton, with a RS energy approximately 9 times greater than the ISBT linewidth for the homogenized structure. This is sufficient to satisfy the strong coupling requirement between the high- k states and the ISBT.

It is important to realize that if the total losses in the system were greater than the degree of interaction between the high- k mode and the ISBT (as determined by the RS energy) no strong coupling would take place. In the semiconductor HMM presented here, the energy losses corresponding to electron scattering and radiative broadening of the ISBT are 6.6 meV and 5 meV respectively. We see in Table I that the smallest magnitude of the RS energy (38 meV) is sufficiently larger than the total energy loss in the system (11.6 meV). As a result, each of the high- k modes strong couples to the ISBT.

Furthermore, upon closer inspection of Table I, we see the magnitude of the RS energy decreases with increasing values of the in-plane wavevector (k_x). This is explained by observing that the maximum amplitude of the electric fields in the growth direction (E_z) also decreases with k_x and the Type II mode number. This is outlined in the inset of Figure 6(a) using the in-plane magnetic fields ($|B_y|$). We use ($|B_y|$) instead of the discontinuous perpendicular electric fields ($|E_z|$) for the sake of clarity. The ISBT, for the coordinate axis used in this paper, requires z-polarized E-fields for the transition to be allowed as a result of orthogonality conditions. The strength of the ISBT is dependent on the magnitude of the electric fields normal to the interface and, as a result, the decreasing E_z field magnitude leads to a decreased ISBT absorption. The decreased strength of the transition leads to reduced coupling with the high- k mode and the overall RS energy is decreased.

IV. STRONG COUPLING IN TYPE II SEMICONDUCTOR HMMS: MULTILAYER REALIZATION

We now validate the EMT calculations of Section III with a practical multilayer approach for the semiconductor HMM. Here, we determine the transmission of the incident radiation through each individual layer of the structure with the transfer matrix method. Determination of optical properties in this fashion is more representative of a structure conceived in fabrication.

Strong coupling behaviour in a practical multilayer realization of the semiconductor HMM shows comparable results to those seen with EMT. Analysis of the transmission spectra of the semiconductor HMM was obtained through the numerical transfer matrix method (Figure 6). The multilayer structure analyzed consists of 5 layers of an 80 nm MQW slab alternated with 5 layers of an 80 nm n^+ -InGaAs semiconductor for a total structure thickness of 800 nm. Note that the total thickness of the structure is the same thickness as the analysis done with the EMT slab in Section III.

Figure 6 shows very good agreement with the EMT dispersions shown in Figure 4, including the mode profile of the high- k modes as well as the strong coupling behaviour with the ISBT. The multilayer structure, however, has a distinct upper cut-off for the high- k modes that was not seen in the EMT structure. At larger wavevector magnitudes the waves begin propagating with wavelengths comparable to the size of the unit cell and no longer interact with the structure as an effective medium. The wavevectors lie at the edge of the Brillouin zone of the periodic lattice and begin to Bragg scatter, leading to an upper limit to the wavevector magnitude of the high- k modes which can propagate in the multilayer structure. The transfer matrix method takes the size of the unit cell into account, and thus in the multilayer semiconductor HMM (Figure 6), a sharp upper cut-off is observed at the point where the wavevector becomes comparable to the unit cell size [31].

Figure 6(b) confirms the strong coupling behaviour in the multilayer semiconductor HMM. The magnitude of the strong coupling in the multilayer structure was extracted by comparing the analytical expression of Equation 12 with the numerical results in the same manner as was done with the EMT slab (Section III). We note that in the multilayer structure only 3 high- k -ISBT polaritons are present in comparison to the 4 seen with the EMT slab of the same thickness due to the upper cut-off wavevector of the multilayer structure. As expected, the maximum RS energy ($\hbar\Omega = 52$ meV) occurs for the first high- k -ISBT polariton for the system, a value approximately 10.5 times greater than the ISBT linewidth.

Again, similar to the EMT slab, we see decreasing values of the RS energy for larger values of the in-plane wavevector (k_x) and increasing high- k -ISBT polariton mode number (Table II). The magnitude of the in-plane

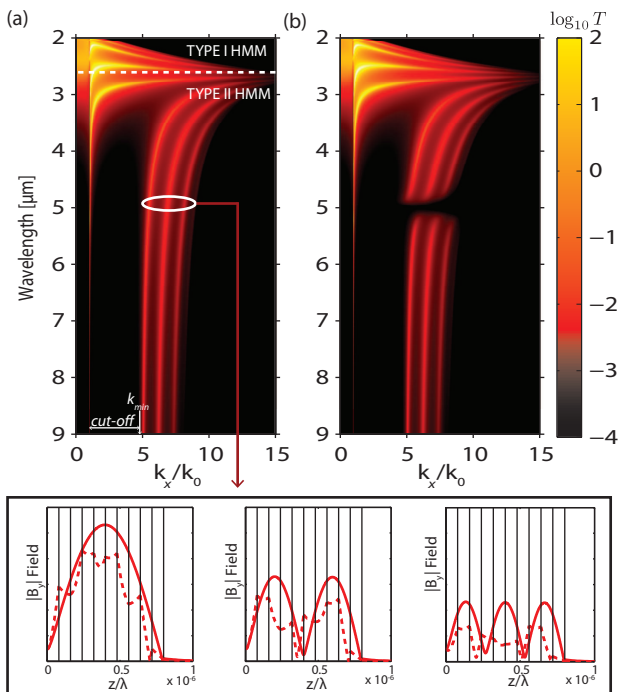


FIG. 6: Transmission of 10 alternating MQW and InGaAs 80 nm layers using the transfer matrix method. (a) Type I and Type II high- k modes of the multilayer structure with intersubband transitions (ISBTs) tuned away from the mode energies. (b) Strong coupling between the ISBT and Type II modes of the multilayer structure at $\lambda_{ISBT} = 5\mu\text{m}$. A series of high- k -ISBT polaritons are formed. In both (a) and (b) the multilayer structure shows strong agreement with the effective medium results of Figure 4. Note that the multilayer structure, in comparison to the homogenized slab, experiences an upper cutoff of the wavevector as it approaches the size of the unit cell. The cut-off region for wavevectors smaller than k_{min} shows a match to EMT (Figure 4). k_0 is the free-space wavevector. Inset of (a) shows relative magnitudes of the in-plane magnetic field ($|B_y|$) at a wavelength of $5\mu\text{m}$ for the first 3 high- k modes of the MQW-InGaAs multilayer (dashed) and homogenized (solid) structure.

magnetic fields (B_y) (inset of Figure 6(a)) also decreases with increasing k_x for the multilayer structure, matching the observations seen with EMT.

V. CONCLUSION

Here, we have proposed a design for an active multilayer semiconductor structure able to achieve hyperbolic

dispersion in the mid-IR. The structure consists of an alternating active dielectric component with embedded quantum wells and a metallic component composed of a degenerately doped semiconductor.

A practical semiconductor HMM can be realized experimentally through fabrication with established techniques such as molecular beam epitaxy. The dispersion profiles of the high- k modes and the ISBT of the structure

TABLE II: Rabi splitting (RS) energy between Type II HMM Modes and the ISBT for the MQW-InGaAs multilayer structure shown in Figure 6. The magnitude of the RS is decreasing with increasing Type II mode number and wavevector, similar to the results seen in Table I for the homogenized MQW-InGaAs slab

High- k ISBT	k_x/k_0 Bounds	RS Energy ($\hbar\Omega$) [meV]
1	4.5-6.2	52
2	6.6-7.6	48
3	7.8-8.8	47

can be determined through angle resolved spectroscopic techniques. This is achieved using p-polarized light that is prism coupled in either the Kretschmann or Otto configuration. Prism coupling is necessary to couple incident light into the high- k modes of the metamaterial. The experimentally measured dispersion profiles can be used to assess the tunability of the RS energy in a practical semiconductor structure. This structure can have potential applications in quantum well infrared photodetectors and tunable intersubband light-emitting devices.

In this paper, we have described strong coupling interactions between the high- k modes of the HMM and the intersubband transitions of the embedded quantum wells with Rabi splitting energies up to 52 meV. The system showed strong coupling behaviour in the effective medium approach as well as a practical structure. The numerical strong coupling dispersion showed strong agreement when compared to a semiclassical analytic expression describing the anti-crossing behaviour of strongly coupled systems. This is the first example of strong coupling behaviour in hyperbolic metamaterials.

- [1] Vladimir M Shalaev. Optical negative-index metamaterials. *Nature Photonics*, 1(1):41–48, January 2007.
 [2] L Menon, W T Lu, A L Friedman, S P Bennett, D Heiman, and S Sridhar. Negative index metamaterials based on metal-dielectric nanocomposites for imaging applications. *Applied Physics Letters*, 93(12):123117, September 2008.
 [3] S Foteinopoulou, E N Economou, and C M Soukoulis.

materials based on metal-dielectric nanocomposites for imaging applications. *Applied Physics Letters*, 93(12):123117, September 2008.

[3] S Foteinopoulou, E N Economou, and C M Soukoulis.

- Refraction in Media with a Negative Refractive Index. *Physical Review Letters*, 90(10):107402, March 2003.
- [4] Zubin Jacob, Leonid V Alekseyev, and Evgenii Narimanov. Optical Hyperlens: Far-field imaging beyond the diffraction limit. *Optics Express*, 14(18):8247–8256, September 2006.
- [5] Zhaowei Liu, Stéphane Durant, Hyesog Lee, Yuri Pikus, Nicolas Fang, Yi Xiong, Cheng Sun, and Xiang Zhang. Far-Field Optical Superlens. *Nano Letters*, 7(2):403–408, February 2007.
- [6] a V Kabashin, P Evans, S Pastkovsky, W Hendren, G a Wurtz, R Atkinson, R Pollard, V a Podolskiy, and a V Zayats. Plasmonic nanorod metamaterials for biosensing. *Nature materials*, 8(11):867–71, November 2009.
- [7] Alexander A Govyadinov and Viktor A Podolskiy. Metamaterial photonic funnels for subdiffraction light compression and propagation. *Physical Review B*, 73(15):155108, April 2006.
- [8] K. Tanaka, E. Plum, J. Y. Ou, T. Uchino, and N. I. Zheludev. Multifold enhancement of quantum dot luminescence in plasmonic metamaterials. *Phys. Rev. Lett.*, 105:227403, Nov 2010.
- [9] Zubin Jacob and Vladimir M Shalaev. Plasmonics Goes Quantum. *Science*, 334(6055):463–464, October 2011.
- [10] Zubin Jacob, Igor I Smolyaninov, and Evgenii E Narimanov. Broadband Purcell effect: Radiative decay engineering with metamaterials. *Applied Physics Letters*, 100(18):181104–181105, May 2012.
- [11] M A Noginov, H Li, Yu. A Barnakov, D Dryden, G Nataraj, G Zhu, C E Bonner, M Mayy, Z Jacob, and E E Narimanov. Controlling spontaneous emission with metamaterials. *Optics Letters*, 35(11):1863–1865, June 2010.
- [12] X Ni, GV Naik, AV Kildishev, Yu Barnakov, Alexandra Boltasseva, and VM Shalaev. Effect of metallic and hyperbolic metamaterial surfaces on electric and magnetic dipole emission transitions. *Applied Physics B*, 103(3):553–558, 2011.
- [13] G Khitrova, H M Gibbs, M Kira, S W Koch, and A Scherer. Vacuum Rabi splitting in semiconductors. *Nature Physics*, 2(2):81–90, 2006.
- [14] Ralf Ameling, Daniel Dregely, and Harald Giessen. Strong coupling of localized and surface plasmons to microcavity modes. *Optics Letters*, 36(12):2218–2220, June 2011.
- [15] A V Rogacheva, V A Fedotov, A S Schwanecke, and N I Zheludev. Giant Gyrotropy due to Electromagnetic-Field Coupling in a Bilayered Chiral Structure. *Physical Review Letters*, 97(17):177401, October 2006.
- [16] Lucio Claudio Andreani, Giovanna Panzarini, and Jean-Michel Gérard. Strong-coupling regime for quantum boxes in pillar microcavities: Theory. *Physical Review B*, 60(19):13276, 1999.
- [17] P Michler, A Kiraz, C Becher, W V Schoenfeld, P M Petroff, Lidong Zhang, E Hu, and A Imamoglu. A Quantum Dot Single-Photon Turnstile Device. *Science*, 290(5500):2282–2285, December 2000.
- [18] Matthew Pelton, Charles Santori, Jelena Vucković, Bingyang Zhang, Glenn S Solomon, Jocelyn Plant, and Yoshihisa Yamamoto. Efficient Source of Single Photons: A Single Quantum Dot in a Micropost Microcavity. *Physical Review Letters*, 89(23):233602, November 2002.
- [19] Peter Lodahl, A van Driel, Ivan S Nikolaev, Arie Irman, Karin Overgaag, Daniël Vanmaekelbergh, and Willem L Vos. Controlling the dynamics of spontaneous emission from quantum dots by photonic crystals. *Nature*, 430(7000):654–657, August 2004.
- [20] S Hughes. Enhanced single-photon emission from quantum dots in photonic crystal waveguides and nanocavities. *Optics Letters*, 29(22):2659–2661, November 2004.
- [21] D J Shelton, I Brener, J C Ginn, M B Sinclair, D W Peters, K R Coffey, and G D Boreman. Strong Coupling between Nanoscale Metamaterials and Phonons. *Nano Letters*, 11(5):2104–2108, May 2011.
- [22] D Steinbach, G Kocherscheidt, M U Wehner, H Kalt, M Wegener, K Ohkawa, D Hommel, and V M Axt. Electron-phonon quantum kinetics in the strong-coupling regime. *Physical Review B*, 60(17):12079–12090, November 1999.
- [23] Joseph R Lakowicz. Radiative decay engineering 3. surface plasmon-coupled directional emission. *Analytical biochemistry*, 324(2):153–169, 2004.
- [24] J Dintinger, S Klein, F Bustos, William L Barnes, and TW Ebbesen. Strong coupling between surface plasmon-polaritons and organic molecules in subwavelength hole arrays. *Physical Review B*, 71(3):035424, 2005.
- [25] J Bellessa, C Bonnand, JC Plenet, and J Mugnier. Strong coupling between surface plasmons and excitons in an organic semiconductor. *Physical review letters*, 93(3):036404, 2004.
- [26] A Christ, SG Tikhodeev, NA Gippius, J Kuhl, and H Giessen. Waveguide-plasmon polaritons: strong coupling of photonic and electronic resonances in a metallic photonic crystal slab. *Physical review letters*, 91(18):183901, 2003.
- [27] DE Chang, AS Sorensen, PR Hemmer, and MD Lukin. Quantum optics with surface plasmons. *arXiv preprint quant-ph/0506117*, 2005.
- [28] Nina Meinzer, Matthias Ruther, Stefan Linden, Costas M Soukoulis, Galina Khitrova, Joshua Hendrickson, Joshua D Olitsky, Hyatt M Gibbs, and Martin Wegener. Arrays of ag split-ring resonators coupled to ingaas single-quantum-well gain. *arXiv preprint arXiv:1009.0693*, 2010.
- [29] DR Smith and D Schurig. Electromagnetic wave propagation in media with indefinite permittivity and permeability tensors. *Physical Review Letters*, 90(7):077405, 2003.
- [30] Viktor A Podolskiy and Evgenii E Narimanov. Strongly anisotropic waveguide as a nonmagnetic left-handed system. *Physical Review B*, 71(20):201101, 2005.
- [31] C L Cortes, W Newman, S Molesky, and Z Jacob. Quantum nanophotonics using hyperbolic metamaterials. *Journal of Optics*, 14(6):63001, June 2012.
- [32] Yu Guo, Ward Newman, Cristian L. Cortes, and Zubin Jacob. Applications of Hyperbolic Metamaterial Substrates. *Advances in Optoelectronics*, 2012(1):1–9, 2012.
- [33] Ward D Newman, Cristian L Cortes, and Zubin Jacob. Enhanced and directional single-photon emission in hyperbolic metamaterials. *JOSA B*, 30(4):766–775, 2013.
- [34] Ivan Iorsh, Alexander Poddubny, Alexey Orlov, Pavel Belov, and Yuri S Kivshar. Spontaneous emission enhancement in metal-dielectric metamaterials. *Physics Letters A*, 376(3):185–187, 2012.
- [35] Lev S Bishop, JM Chow, Jens Koch, AA Houck, MH Devoret, E Thuneberg, SM Girvin, and RJ Schoelkopf. Non-linear response of the vacuum rabi resonance. *Nature Physics*, 5(2):105–109, 2008.

- [36] Yifu Zhu, Daniel J. Gauthier, S. E. Morin, Qilin Wu, H. J. Carmichael, and T. W. Mossberg. Vacuum rabi splitting as a feature of linear-dispersion theory: Analysis and experimental observations. *Phys. Rev. Lett.*, 64:2499–2502, May 1990.
- [37] J Kasprzak, S Reitzenstein, EA Muljarov, C Kistner, C Schneider, M Strauss, S Höfling, A Forchel, and W Langbein. Up on the jaynes-cummings ladder of a quantum-dot/microcavity system. *Nature materials*, 9(4):304–308, 2010.
- [38] Brahim Lounis and Michel Orrit. Single-photon sources. *Reports on Progress in Physics*, 68(5):1129, 2005.
- [39] Anthony J Hoffman, Leonid Alekseyev, Scott S Howard, Kale J Franz, Dan Wasserman, Viktor A Podolskiy, Evgenii E Narimanov, Deborah L Sivco, and Claire Gmachl. Negative refraction in semiconductor metamaterials. *Nature Materials*, 6(12):946–950, December 2007.
- [40] Jonathan Plumridge and Chris Phillips. Ultralong-range plasmonic waveguides using quasi-two-dimensional metallic layers. *Physical Review B*, 76(7), August 2007.
- [41] V Agranovich, M Litinskaia, and D Lidzey. Cavity polaritons in microcavities containing disordered organic semiconductors. *Physical Review B*, 67(8), February 2003.
- [42] M Zaluzny and C Nalewajko. Coupling of infrared radiation to intersubband transitions in multiple quantum wells: The effective-medium approach. *Physical Review B*, 59(20):13043, 1999.
- [43] Lukas Novotny. Strong coupling, energy splitting, and level crossings: A classical perspective. *American Journal of Physics*, 78(11):1199, 2010.
- [44] Dimitri Dini, Rüdiger Köhler, Alessandro Tredicucci, Giorgio Biasiol, and Lucia Sorba. Microcavity Polariton Splitting of Intersubband Transitions. *Physical Review Letters*, 90(11):1–4, March 2003.
- [45] Jonathan Plumridge, Edmund Clarke, Ray Murray, and Chris Phillips. Ultra-strong coupling effects with quantum metamaterials. *Vacuum*, 146:406–408, 2008.
- [46] M S Skolnick, T A Fisher, and D M Whittaker. Strong coupling phenomena in quantum microcavity structures. *Semiconductor Science and Technology*, 13(7):645–669, July 1998.
- [47] R Houdré, R P Stanley, U Oesterle, M Ilegems, and C Weisbuch. Room-temperature cavity polaritons in a semiconductor microcavity. *Physical Review B*, 49(23):16761–16764, June 1994.
- [48] Harish N S Krishnamoorthy, Zubin Jacob, Evgenii Narimanov, Ilona Kretzschmar, and Vinod M Menon. Topological Transitions in Metamaterials. *Science*, 336(6078):205–209, April 2012.